Effect of operating conditions on the hydrodynamics in fountain confined conical spouted beds

Mikel Tellabide*, Idoia Estiati, Aitor Atxutegi, Haritz Altzibar, Martin Olazar

Department of Chemical Engineering, University of the Basque Country UPV/EHU, P.O. Box 644, E48080 Bilbao (Spain).

Abstract

Spouted bed stability and operation is greatly affected by particle features. Accordingly, the hydrodynamic behaviour of conical spouted beds has been studied for fine particles differing in size and density in a wide range of inlet air flow rates. This knowledge is essential for a successful scaling up and industrial implementation of the spouted bed. Therefore, the effect air velocity and solid properties (density and size) have on local solid velocity has been ascertained in a fountain confined conical spouted bed using a borescope technique (Particle Tracking Velocimetry, PTV) applied to several bed configurations. The results show a close relationship between the inlet air velocity and the local solid velocity, with the gas-solid contact being especially vigorous in the configurations without draft tube and with the open-sided draft tube. The solid circulation flow rate is lowest when a nonporous draft tube is used due to the low solid vertical velocities in the

*Corresponding author
Email address: mikel.tellabide@ehu.eus (Mikel Tellabide)

annulus, even at high air flow rates. Nevertheless, vertical velocities in the annular zone increase when particle size and density are increased, although these velocities are lower in the spout and fountain regions due to the higher momentum exchange required for their acceleration.
Keywords:
Fine particles, particle velocity, spouting regime, solid properties, conical spouted bed, fountain confiner

---

1. Introduction

The spouted bed is a well-known gas-solid contact regime for the treatment of coarse and granular particles (greater than $1\,mm$), for which fluidized beds provide unsatisfactory results. Its main characteristic feature is the cyclic movement of the particles in the bed, which differs from any other gas-solid contact regime. Nevertheless, one of the main drawbacks of this technology lies in the problems involving scaling up [1, 2], which is due to the non-linear nature of parameters governing spouted bed performance.

In order to address this issue, different spouted bed variants have been proposed in the literature, as are conical [3], cylindrical [4], mechanical [5], two-dimensional [6] and rectangular [7] spouted beds. Despite the great variety of geometries, none of them have entirely solved the problem of scaling up. The conical spouted bed is one of the most interesting designs, as it combines the features of cylindrical spouted beds (low operating pressure drop) [8] with the conical shape that ensures operation stability in a wide

range of gas flow rates and configurations [9].

Conical spouted beds have proven to perform successfully in many applications, such as steam gasification [10], coating [11], drying [12], combustion [13] or pyrolysis [14]. Usually, these applications involve the use of a bed made up of inert particles, apart from the active bed (catalyst or any other material), in order attain stable spouting and efficient heat transfer. In most of the cases, the overall hydrodynamic behaviour of the bed is heavily influenced by these inert particles. Nevertheless, the main operating limitations in spouted beds are related to the ratio of inlet diameter to particle diameter, D_0/d_p, which cannot be higher than $20-30$, and the maximum spoutable bed height [1]. Olazar et al. [2] noted that, although the mentioned D_0/d_p range bed may be extended to 60 under certain operating conditions, these limitations also apply to conical spouted beds.

The common solution to operate with fine particles without inlet restrictions ($D_0/d_p > 20-30$) lies in the use of draft tubes [15]. This type of internal device ensures spouting regime, but reduces gas-solid contact [8, 16], and therefore the efficiency of the technology. Recently, a novel internal device called fountain confiner was proposed [17], which allows operating with fine and ultrafine particles without any draft tube. Furthermore, it ensures stable operation for D_0/d_p ratios of up to 1000 [18, 19, 20]. As reported in a previous paper [19], the characteristic curves ($\Delta P\, vs.\, u$) obtained operating with fine particles and fountain confiner differ considerably from conventional ones. In fact, new spouting regimes are observed as the air velocity is increased and

so the gas-solid contact time is changed.

The relationship between air velocity and pressure drop provides basic information about the global behaviour of the system, and therefore allows monitoring the spouting regimes. However, detail information about local properties is required in order to understand the gas and solid flow patterns in the bed. Thus, the acquisition of these data has been proposed based on a number of particle tracking techniques, which are classified as intrusive and non-intrusive methods. In the former, fiber-optic methods [21] are most commonly used to measure particle velocity and bed voidage [22]. Nevertheless, some authors are skeptical about the use of intrusive methods stating that these types of probes disturb the local flow. Thus, a great variety of non-intrusive methods, such as gamma-ray computed tomography [23], magnetic resonance tomography [24] or particle image velocimetry (PIV) [25] have been reported in the literature. PIV technique is a very useful measurement method due its simplicity, but half-column contactors must been used. Therefore, an intrusive PTV technique was proposed by our research group in a previous study, in which it was demonstrated that it is a suitable measuring technique due to the high accuracy of the results (an error lower than 10%) [26] and flexibility of the set-up.

The minimum spouting velocity (u_{ms}) is a relevant operating parameter, but most applications operate at higher velocities than the minimum one. Furthermore, gas velocity highly affects the hydrodynamics of spouted beds, as changes in this parameter may lead to modification in gas and solid flow

patterns in the bed. Therefore, the main aim of this study is to monitor and analyze particle velocities in fine particle beds. The study covers different configurations of fountain confined conical spouted beds, in which operation has been carried out in a wide rage of air velocities (or spouting regimes) and using solids differing in size and density.

2. Experimental

2.1. Equipment

Experimental runs have been carried out in a pilot plant consisting of a blower, flow meter, pressure drop gauge, filter and cyclone, which are described in detail in a previous paper [19]. A contactor made of polyethylene terephthalate has been used (Figure 1a) with the following geometric factors: column diameter (D_C), $0.36\,m$; contactor angle (γ), 36°; height of the conical section (H_C), $0.45\,m$; and base diameter (D_i), $0.06\,m$. The static bed height (H_0) and the gas inlet diameter (D_0) used in all the runs are $0.20\,m$ and $0.04\,m$, respectively.

2.2. Draft tubes

This contactor is designed to fit different draft tubes at the inlet of the conical section. Thus, three different configurations have been used, as are the one without draft tube, and those equipped with open-sided and non-porous draft tubes. All the tubes are made of stainless steel, Figures 1b and 1c, with the main dimensions been as follows: length of the tube (L_T),

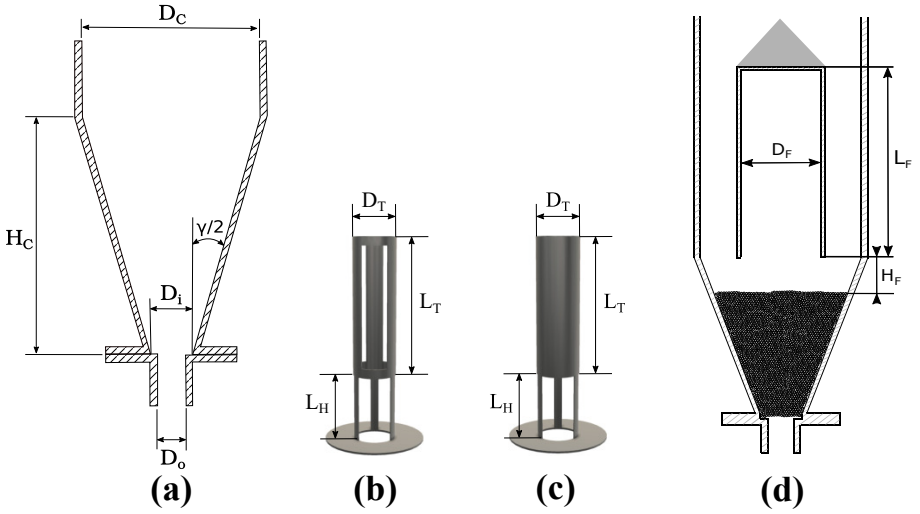

Figure 1: Geometric factors of the (a) conical contactor, (b) open-sided draft tube, (c) nonporous draft tube, and (d) fountain confiner.

0.20 m; entrainment height (L_H), i.e., distance between the gas inlet nozzle and the lower end of the tube, 0.07 m; diameter of the tube (D_T), 0.04 m; and aperture ratio (AR), i.e., the fraction of the lateral surface area opened for gas and solid cross flow, with its values being 57% for the open-sided draft tube and 0% for the nonporous one.

2.3. Fountain confiner

Fine particle operation require the use of a fountain confiner (Figure 1d) in order to attain stable spouting and avoid particle entrainment. This internal device is a cylindrical pipe made of polyethylene terephthalate with the upper end closed to avoid gas and solids leaving the contactor through its top. It has a cone shaped cap on the top to avoid deposition of solids on the outside of the device. The diameter (D_F) and length (L_F) of the fountain

confiner are 0.20 and 0.50 m, respectively. Furthermore, the distance between the bed surface and the lower end of the device (H_F) is 0.06 m, Figure 1d.

2.4. Materials

In order to study the effect of particle size, two fractions of siliceous sand were used, and the effect of particle density was explored by spouting pine sawdust of the same size as the coarse sand. The particle size distribution and average sizes were obtained in a CISA RP 200 N sieve shaker using mesh sizes of 100, 200 and 300 μm and confirmed through laser diffraction in a Mastersizer 2000. Thus, the average size values are 0.155 and 0.246 mm for sand, and 0.244 mm for sawdust. The densities of sand and sawdust particles, obtained in an Autopore 9220 mercury porosimeter (Micromeritics), are 2390 $kg\,m^{-3}$ and 496 $kg\,m^{-3}$, respectively.

2.5. Operating conditions

Table 1 shows the regimes and air velocities used with the configurations and particles studied. As observed, sand particles of $d_p = 0.246\,mm$ have been taken as the base case and certain runs changing particle size and density have been conducted in order to analyze their influence. In the case of the configuration without tube, given the narrow stability range, only a couple of air velocities were chosen, as are one corresponding to the minimum spouting and the other one to the minimum for full spouting. Once internal devices were added this range was considerably widened, allowing for more than one air velocity to be used in the full spouting regime. Finally, in

order to analyze the effect of solid properties on particle velocity, a finer sand ($d_p = 0.155\,mm$) and sawdust with a similar size ($d_p = 0.244\,mm$) as the base case were used. These runs were carried out in the configuration with the open-sided tube at the minimum spouting velocity, as it is the one ensuring steady spouting and suitable solid flow in a wide range. The minimum spouting velocities corresponding to the three runs differing in size and density are 3.42, 2.21 and $1.43\,m\,s^{-1}$ for the sands of $d_p = 0.246$ and $0.155\,mm$ and the sawdust of $d_p = 0.244\,mm$, respectively.

2.6. Experimental procedure

A high speed camera fitted to a borescopic system (Figure 2a) has been used to track particles inside the spouted bed and measure their velocity. The camera is an AOS S-PRI (AOS Technologies AG) with a maximum recording resolution of 900×700 pixels and a maximum frame rate of 16500 fps with reduced resolution. Furthermore, a continuous light source connected to the borescope through an optical fibre is used to light the recording zone. The optical set-up is displaced by a set of sliders (Figure 2b), which enable positioning the borescope measuring tip anywhere in the contactor. More details about the optical and borescopic systems are provided in a previous paper [26].

Particle velocity profiles have been determined, with the axial one corresponding to the axis along the spout and fountain core, and the radial ones to several bed levels, in which solid velocity changes from positive (spout

Table 1: Regimes and air velocities analysed in the configurations studied.

Configuration	**Regime**	**Air velocity** ($m\,s^{-1}$) Sand $0.246\,mm$	Sand $0.155\,mm$	Sawdust $0.244\,mm$
Without tube	Spouting	3.86 (u_{ms})	—	—
	Full spouting	12.80 ($3.31u_{ms}$)	—	—
Open-sided tube	Spouting	3.42 (u_{ms})	2.21 (u_{ms})	1.43 (u_{ms})
	Full spouting	8.06 ($2.35u_{ms}$)	—	—
		21.93 ($6.40u_{ms}$)	—	—
Nonporous tube	Spouting	2.54 (u_{ms})	—	—
	Full spouting	5.08 ($2u_{ms}$)	—	—
		7.63 ($3u_{ms}$)	—	—
		21.86 ($8.60u_{ms}$)	—	—

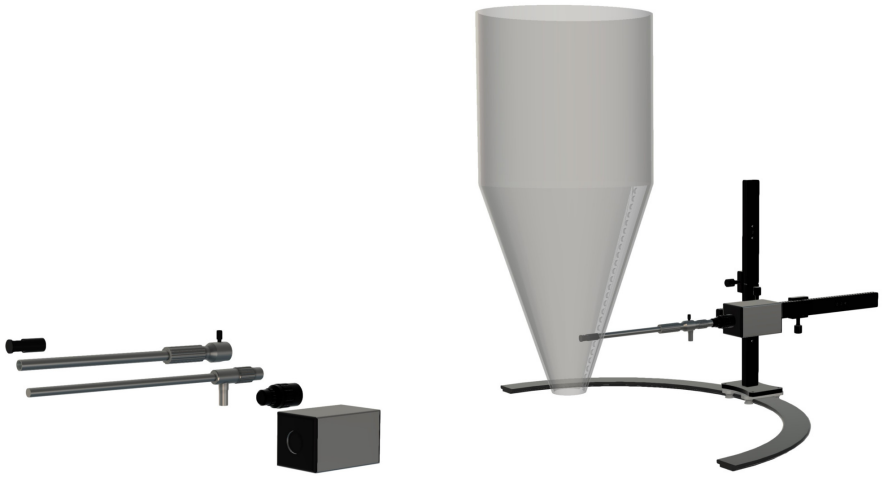

(a) (b)

Figure 2: Experimental set-up of (a) the borescope assembly and (b) the optical system.

and fountain core regions) to negative values (annular and fountain periphery regions). It should be noted that all the velocities measured correspond to the vertical component. This technique has been designed to take the measurements in front of the borescope tip, where there is no disturbance in the bed, as any perturbation would occur behind the device.

The radial measurements have been carried out at four levels in the spout and annulus, and four levels in the fountain region. Thus, the bed levels analysed from the bed bottom to the fountain top are as follows: 0.03, 0.11, 0.15, 0.20, 0.24, 0.30, 0.53 and $0.73\,m$, for a static bed height (H_0) of $0.20\,m$. The tip of the borescope is placed at the first measuring point (contactor or confiner wall, depending on the level to be analysed) and four recordings are carried out at different times. Then, the borescope tip is displaced step-by-step along the radial direction to the next measuring points (every

centimetre) until the axis of the contactor is reached. This procedure has been repeated at all the bed levels.

2.7. Particle tracking technique

Based on the optical system described, solid velocities are calculated through the detection of the solid optical flow. Nevertheless, the packing condition in the different regions in the spouted bed is very different, and this is evidenced on the images captured. Accordingly, the particle identification method must be adapted to account for these differences in voidage from dense (annulus) to dilute (spout and fountain) zones. In the former, particles descend in a moving bed and individual particle rotations are negligible. Therefore, the Farneback pyramidal algorithm [27] from OpenCV has been found to be especially suitable to measure the average edge movement. In the dilute regions (spout and fountain), once dynamic histogram equalization and canny edge detection have been applied, closed regions are identified as individual particles in consecutive frames. Finally, minimization of the total solid displacement allows pairing particles in consecutive frames and calculating the optical displacement. Considering that spouted beds have mainly vertical solid displacement in the annulus, spout and most of the fountain region, this optical displacement has been related to the solid velocity based on pixel distance and recording frame rate.

3. Results

3.1. Particle flow pattern in the annular zone

As stated in a previous paper [28], the flow pattern of fine particles in fountain confined conical spouted beds is characterized by oscillatory movements. This trend is observed in the three regions of the spouted bed, but is in the annulus where it is most evident. Figures 3a-c show the evolution of particle velocity with time under different air velocities in each configuration.

As shown in Figures 3a-c, particles move downwards along the annulus following an oscillatory trend. This applies to the three configurations and all the inlet air velocities analyzed. Nevertheless, there are great differences in the oscillations depending on the configuration [28]. Thus, the particles oscillate from upward to downward velocities in the configurations without tube and with open-sided tube (Figures 3a and 3b), whereas they oscillate from zero to a maximum downward velocity in the configuration with non-porous tube, Figure 3c. Furthermore, the effect of the inlet air flow rate on the particle velocity oscillation is different depending on the configuration.

In the case of the configuration without tube (Figure 3a), the amplitude of the signal oscillation increases as air velocity is increased, which is explained by the higher percolation of the air into the annulus. Therefore, particle movement is more vigorous in the annulus and they travel longer distances (upwards and downwards) as the inlet air velocity is increased, which is clear evidence of an improvement in the gas-solid contact in this zone and so in heat and mass transfer rates.

A similar trend is observed in the open-sided configuration (Figure 3b)

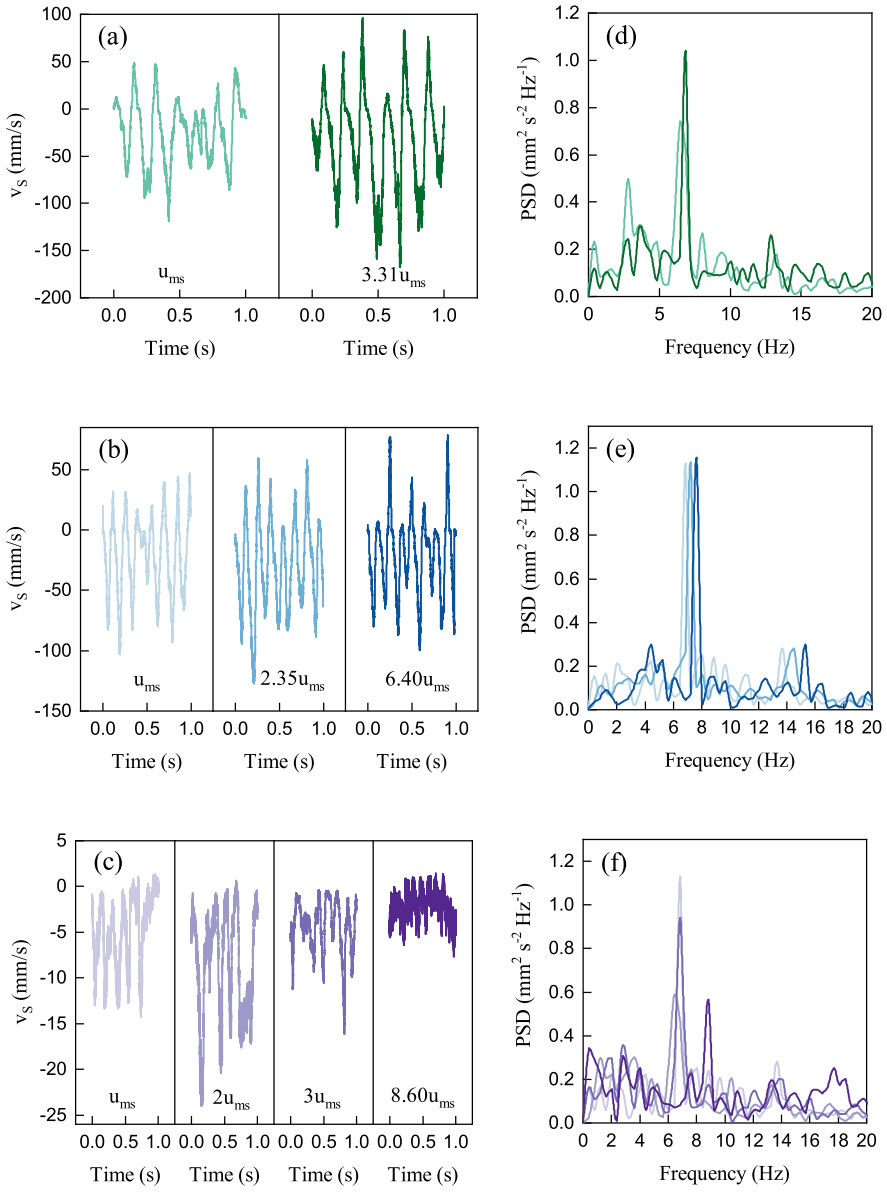

Figure 3: Vertical particle velocities vs. time in the annulus of the configurations (a) without tube and with (b) open-sided and (c) nonporous tubes, and their corresponding power spectral densities vs. frequency, (d), (e) and (f), respectively. Measurements under different air velocities at $r/R = 0.84$ and bed level of $H = 0.20\,m$.

within a given range from the minimum spouting velocity, although less pronounced than in the configuration without tube. Thus, an increase in air velocity to 2.35 times the minimum one favors the oscillatory movement, but a further increase to 6.40 u_{ms} leads to a decrease in the oscillation amplitude, especially in the downward side. This is again explained by the high air percolation from the spout into the annulus for high inlet air flow rates, which in this case may hinder the downwards solid circulation. These results are consistent with the hydrodynamic curves obtained in a previous paper [19], since 2.35 times the minimum spouting velocity corresponds to the beginning of the full spouting regime, which is evidenced with a peak in pressure drop value in the characteristic curve. When the inlet air velocity is increased much further, the pressure drop decreases, which is related to a reduction in solid circulation due to the preferential air flow through the spout. Therefore, the beginning of this regime (full spouting) corresponds to the most vigorous gas-solid contact in the whole operational curve.

Finally, the nonporous tube configuration (Figure 3c) only shows downward movement in the annular region, i.e., particles travel all the time downwards according to oscillations involving acceleration/deceleration/stagnation [6]. In this configuration, the central tube directs the inlet air through the spout and only a small fraction diverts into the annulus through the entrainment zone, which leads to a poorer gas-solid contact and low solid circulation than in the other configurations. When the inlet air flow rate is double the minimum spouting one, the amplitude of the particle velocity signal is ap-

proximately double. Nevertheless, as velocity is increased above this point the amplitude decreases. In fact, there is hardly any oscillation in the annulus particle velocity for an inlet velocity of 8.60 u_{ms}, which is because most of the air is directed through the spout, resulting in a very packed annular region [29].

In addition, Figures 3d-f show the dominant frequency when each configuration is operated at different air velocities. In the systems without tube (Figure 3d) and with the open-sided one (Figure 3e), the dominant frequency increases slightly as the inlet air velocity is increased. Several authors [6, 29, 30] reported a similar trend, in which the oscillations in the spout propagate from the bottom to the surface of the bed. Moreover, they state that a solid preferential incorporation into the spout occurs in the neck of this zone [6], in which particles incorporate massively as clusters. Nevertheless, Gao et al. [31] report a decrease in frequency when air flow rate is increased, which they relate to bubble eruption frequency. In our systems operated with fine particles, the oscillation frequency increases as air velocity is increased, independently of the oscillation amplitude. It seems that this increase in the dominant oscillation frequency is related to the decrease in the clustering behavior of the particles in the bed as the inlet air velocity is increased.

In the case of the nonporous configuration, a similar dominant frequency value is obtained up to three times the minimum spouting velocity (Figure 3f), but sharply increases at high air velocities ($8.6u_{ms}$). The decrease in

the amplitude of the signal, together with the increase in the dominant frequency, are evidence of low particle clustering at these high flow rates. Visual observation of the particles in the fountain also suggest a higher solid fluidity at higher air flow rates.

Figure 4 shows the evolution of particle velocity in the annulus and the dominant frequency for different particle sizes and materials when the open-sided draft tube configuration is used. As shown in Figure 4a, all types of particles show an oscillatory velocity pattern with downward and upward velocities. Nevertheless, the biggest sand fraction shows the highest particle velocity values, i.e., oscillation amplitude is closely related to particle size, and therefore to the overall downward particle flow. Regarding the dominant frequency, Figure 4b shows no influence of particle size, but a lighter material, such as sawdust, leads to a significantly increase in the oscillation frequency. This result suggests that oscillatory patterns with fine particles depend mostly on solid density. Studies in the literature [29, 30] reported that the dominant frequency reduces as the particle size is increased, but they correspond to coarse particles, for which the clustering process hardly applies.

3.2. Radial particle velocity profiles

Average particle velocities have been calculated from the particle velocity fluctuation data at different radial positions and they have been plotted against the dimensionless radius (radius of the measuring point divided

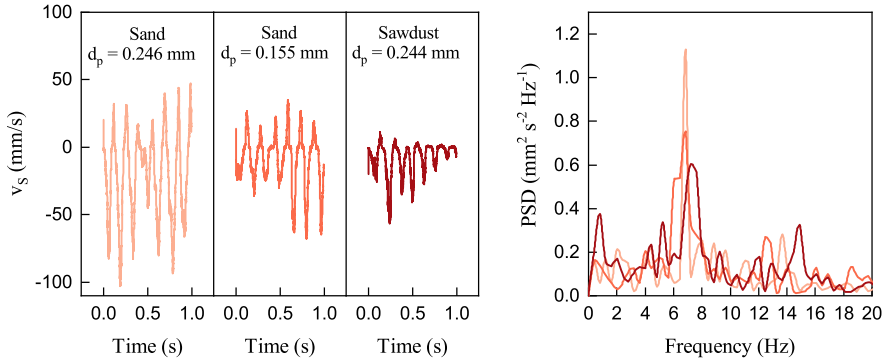

Figure 4: (a) Vertical particle velocity vs. time and (b) power spectral density vs. frequency in the annulus at $r/R = 0.84$ and bed level of $H = 0.20\,m$ in an open-sided draft tube operated with particles differing in size and density.

by the total radius on the measuring plane). Thus, radial particle velocity profiles have been obtained at different heights for the three configurations studied. Figure 5 shows the profiles at the different spouted bed regions and air velocities for the configurations studied.

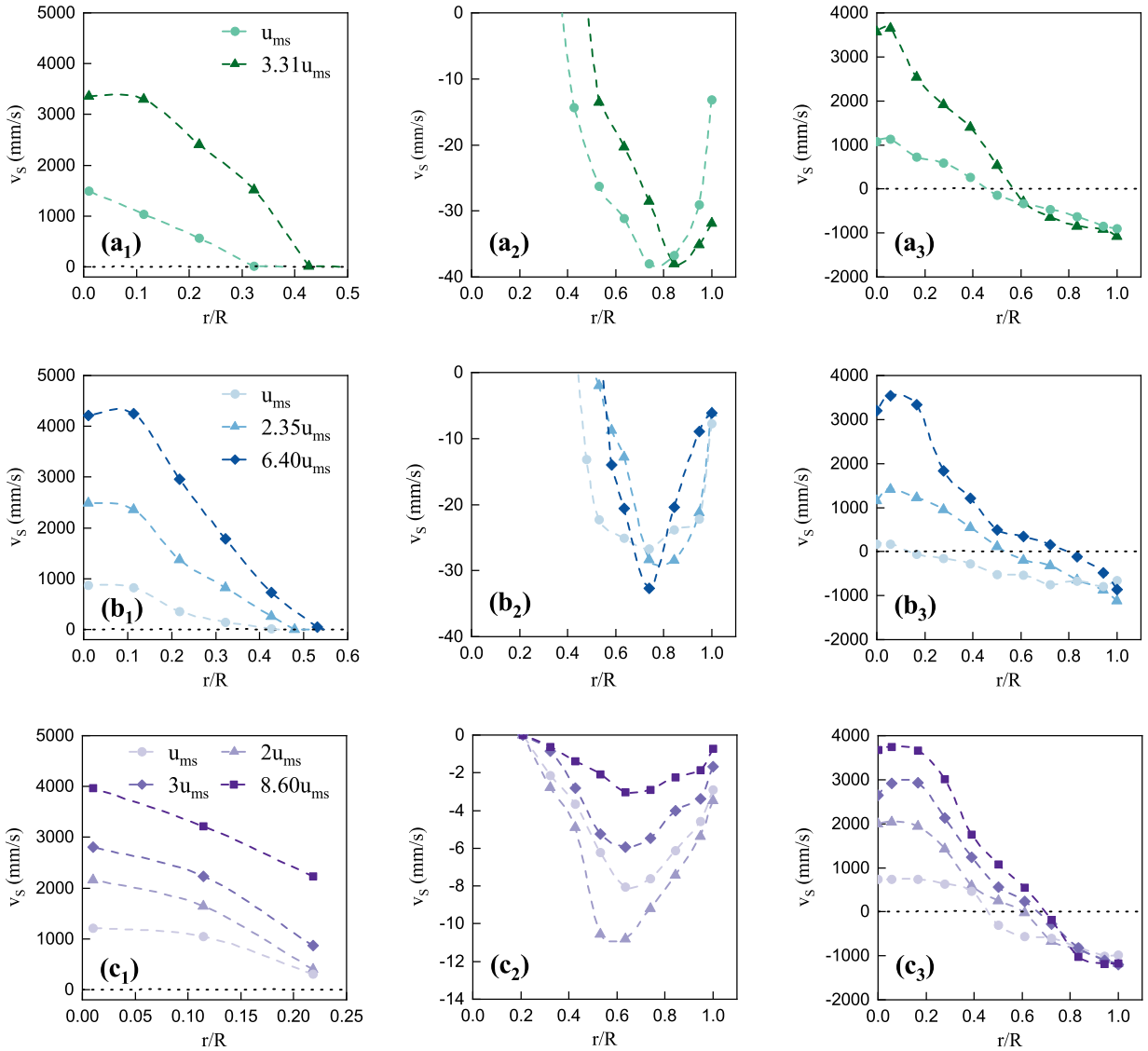

Figure 5: Radial particle velocity profiles in the (a_1, b_1, c_1) spout ($H = 0.20\,m$), (a_2, b_2, c_2) annulus ($H = 0.20\,m$) and (a_3, b_3, c_3) fountain ($H = 0.30\,m$) for the configurations (a_1, a_2, a_3) without tube and with (b_1, b_2, b_3) open-sided tube and (c_1, c_2, c_3) nonporous tube at different air velocities.

As shown in Figures $5a_1$, b_1 and c_1, all the radial profiles obtained in the spout show the same trend, i.e., the particle velocity increases as the axis is approached. This trend has been reported in the literature by several authors [32, 22, 33, 34, 35]. In the configurations without draft tube (Figure $5a_1$) and open-sided tube (Figure $5b_1$), as the air velocity is increased the peak particle velocity is not located at the axis itself, but close to it, which is related to a expanding spout at that bed level under the conditions studied. However, using a nonporous tube (Figure $5c_1$), most of the air is directed through the tube and the spout expansion is limited by the wall of the device. Therefore the peak particle velocity is located at the axis itself. Furthermore, the velocity on the inside wall of the tube is not zero, especially for inlet air velocities higher than the minimum one.

Figures $5a_2$, b_2 and c_2 show the radial particle velocity profiles at different air velocities in the annular zone for the three configurations studied. In the configuration without draft tube (Figure $5a_2$), a high air velocity led to an increase in particle velocity near the contactor wall, but the general trend is very similar for both air velocities [33]. However, due to the great expansion of the spout at high air velocities, particle velocities close to the spout wall are lower than those corresponding to the minimum spouting. Thus, as Djeridane et al. [36] reported, the annular section is reduced as the air velocity is increased, which leads to higher velocities close to the contactor wall and lower close to the spout.

A similar trend as that observed for the configuration without draft tube

is found for the configuration with open-sided tube (Figure $5b_2$) when air velocity is increased to 2.35 times the minimum one, i.e., from the minimum for spouting (u_{ms}) to the minimum for full spouting ($2.35u_{ms}$). Nevertheless, this trend undergoes changes when the air velocity is increased to very high values (6.40 times the minimum one). Thus, the peak is more pronounced and the downward particle velocity is considerably lower from the peak position to the wall.

In the configuration with a nonporous draft tube (Figure $5c_2$), the radial profiles in the annulus corresponding to the different air velocities show a similar trend, i.e., particle velocities increase until a peak is reached, and they then decrease as particles approach the contactor wall. As mentioned in Figure 3c, the velocity of particles descending along the annulus increases as air velocity is increased to $2u_{ms}$, but higher inlet air velocities decrease particle velocity. A close observation of the fountain allows inferring that particle clustering is especially evident up to $2u_{ms}$, which is evidence that particle clusters are incorporation into the spout. Nevertheless, higher inlet air flow rates lead to a more uniform particle flow. According to Ji et al. [29], who used fine particles with a nonporous draft tube, as the air velocity is increased the solid circulation rate decreases due to some particles being carried back into the annular region (in the entrainment zone) by the substantial gas percolation, thus creating a more homogeneous and dilute solid flow inside the draft tube when high velocities are used than when low air velocities are used.

Finally, all the radial profiles obtained in the fountain zone follow a similar parabolic pattern (Figures $5a_3$, b_3 and c_3). In the configurations without draft tube (Figure $5a_3$) and with nonporous tube (Figure $5c_3$), the particle downward velocity in the fountain periphery slightly increases with air velocity, but the opposite trend is observed for open-sided tubes (Figure $5b_3$). The core of the fountain (particle upward zone) increases in all cases as the inlet air flow rate is increased, but this is especially evident in the configurations with the open-sided tube. Although in the configuration with the nonporous draft tube the spout diameter does not change because is limited by the tube diameter, the core of the fountain increases slightly as the inlet air flow rate is increased.

3.3. Axial particle velocity profiles

Figure 6 shows the particle velocity profiles along the axis of the contactor for the three configurations studied under different hydrodynamic conditions; that is, different inlet air flow rates based on the minimum one.

As shown in Figure 6, a general trend is observed in all the profiles, i.e., particles accelerate in the spout up to a peak velocity, and subsequently decelerate in the fountain core. Moreover, another general trend observed in Figure 6 is that particle velocities are higher as the inlet air velocity is higher [6, 30, 33]. However, it is noteworthy that high air velocities ($3.31u_{ms}$, corresponding to the full spouting regime) in the configuration without draft tube (Figure 6a) lead to particle acceleration up to the bottom of the confiner

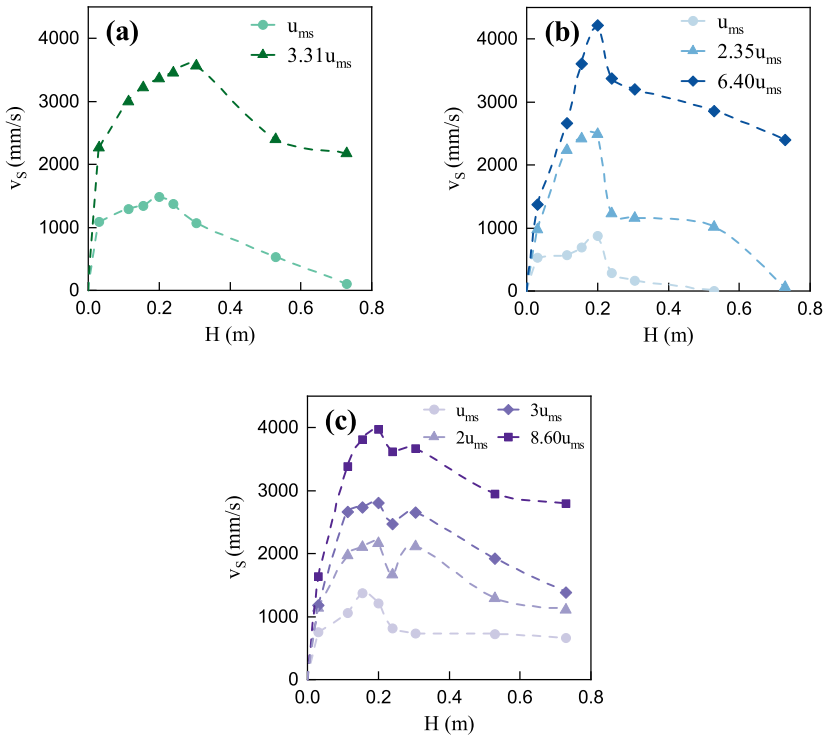

Figure 6: Particle velocity profiles along the axis for the configurations (a) without tube and with (b) open-sided and (c) nonporous tubes, at different air velocities.

($0.10\,m$ above the bed surface), and they then are decelerate as they move upwards along the confiner. Furthermore, high particle velocities are registered at the top of the confiner (around $2\,m\,s^{-1}$). The peak velocity in this configuration shifts to higher positions as the inlet air velocity is increased, which has been explained in the literature by the high drag force of the air [36]. However, in the configuration with the nonporous tube operated at the minimum spouting velocity, particles begin to decelerate in the upper half of the bed (above $0.15\,m$) due to the low air velocity required to open the spout in this configuration [28]. When open-sided draft tubes are used (Figure 6b), particles accelerate up to bed surface at all air velocities studied. Nevertheless, it is noteworthy that it is the only configuration in which the fountain does not reach the upper wall of the confiner at the minimum spouting velocity. This is because open-sided tubes confer high stability upon the system with a great solid circulation, with the minimum air flow rate required for spouting being lower than in the configuration without draft tube.

Finally, as shown in Figure 6c, a local minimum particle velocity is observed in the longitudinal particle velocity profile ($H = 0.24\,m$) when operating in the configuration with the nonporous tube and air velocities above the minimum one. These minima are located in the gap beteween the bed surface and the lower end of the confiner, and might be a consequence of particles leaving the confiner interfering with particles ascending through the spout. As the air flow rate is increased, this interference is reduced, as the gas retains enough momentum to push particles through this stretch.

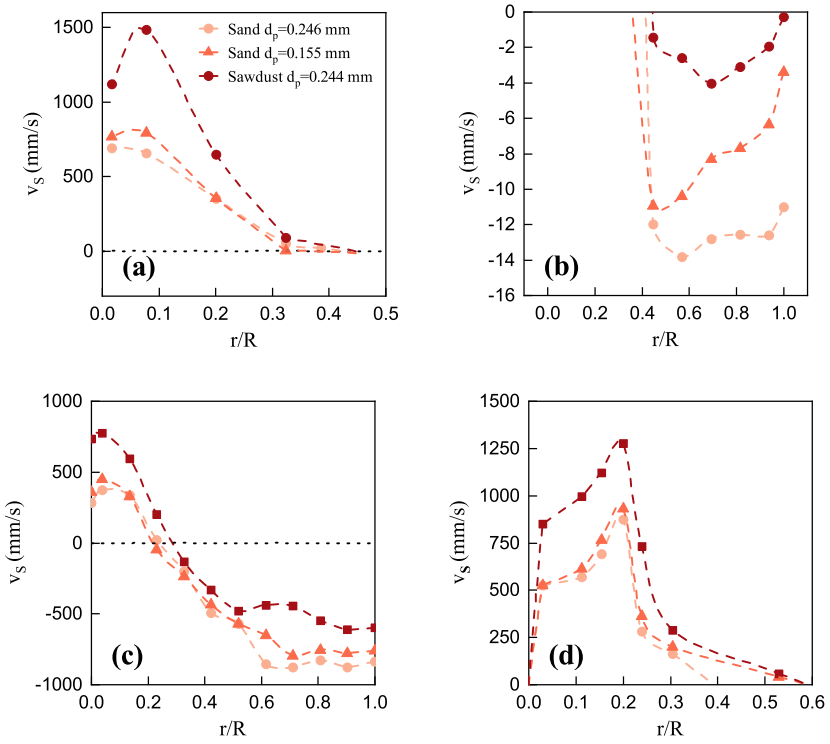

Figure 7: Radial particle velocity profiles in the (a) spout ($H = 0.15\,m$), (b) annulus ($H = 0.15\,m$) and (c) fountain ($H = 0.24\,m$); and (d) particle velocity profiles along the axis for sand beds differing in size and a sawdust bed, in the configuration with open-sided draft tube at the minimum spouting velocity.

3.4. Effect of particle properties

The effect of solid properties has been analysed using particles differing in size and density. Figure 7 shows the radial and longitudinal particle velocity profiles of two sand beds differing in particle size and one sawdust bed.

As shown in Figure 7, similar particle velocity profiles as those shown in Figures 5-6 have been obtained when beds made up of particles differing in size and density have been used. Regarding the spout (Figure 7a), sawdust

particles rise much faster ($1.5 - 2$ times) than sand ones [37], especially in positions near the axis. A comparison of the profiles obtained for beds differing in size shows that its influence is smaller than that of density [38], i.e., the smaller particles ($dp = 0.155\,mm$) have slightly higher velocities than the bigger ones ($dp = 0.255\,mm$) near the spout axis [39, 32], but similar or slightly lower velocities in positions near the spout wall. These results are mainly explained by the lower particle density of sawdust and the higher air-particle momentum exchange with the smaller particles.

The opposite trend is observed in the annular zone (Figure 7b), i.e., sand particles tend to move faster than sawdust ones due to their bigger mass. However, the trends of the profiles are similar in all cases, except that the peak particle velocity is located closer to the spout wall as the particle density is increased.

The radial particle velocity profiles in the fountain (Figure 7c) are similar to those shown in Figures $5a_3$, b_3 and c_3. A more detailed analysis shows that sawdust particles have the greatest particle velocity in the fountain core and the lowest one in the periphery. However, sand beds differing in size show similar radial particle velocity profiles in the fountain core (Figure 7c), as was the case in the spout (Figure 7a). Furthermore, there is only a slight difference between the velocity values corresponding to the smaller and bigger sand particles, except in the fountain periphery close to the contactor wall (in the gap between the bed surface and the lower end of the confiner). As previously explained for the spout (Figure 7a), the upward particle velocity

in the fountain core increases as the particle size is smaller due to the high gas-solid momentum exchange with small particles. The opposite trend is observed in the fountain periphery due to the greater gravitational force of the bigger particles. Moreover, as determined in a previous paper [20], the effect of solid density is more influential than that of particle size on the minimum spouting velocity, and the same applies to particle velocities, i.e., density is more influential than size, when both are changed in a ratio of approximately two. Accordingly, for similar hydrodynamic conditions, a greater spout and fountain core expansion is observed for the sawdust bed than for sand beds.

Figure 7d shows the particle velocity profile along the axis for particles differing in size and density. The velocity profiles for all the different particles show the same trend, i.e., the particles accelerate along the spout, they then decelerate in the fountain until they reach null velocity, and finally start descending in the fountain periphery. Moreover, as shown in Figures 6 and 7d, the maximum acceleration is observed at the bottom of the cone. Concerning the effect of particles properties, all the facts mentioned for the radial profiles, Figures 7a and 7c, apply to the profiles along the axis.

4. Conclusion

This study shows that air velocity and solid properties significantly affect particle velocity, and therefore spouted bed hydrodynamics. Accordingly, detailed information concerning their influence is essential for the scaling up

of this technology.

In the case of the configuration without draft tube, an increase in the inlet air velocity over the minimum one favours solid circulation and gas-solid contact. Nevertheless, high air flow rates lead to mixed regimes rather than spouting ones. This problem is solved by the insertion of a draft tube, but, even in this case, excessively high air velocities over the minimum one lead to a decrease in solid circulation. For the configurations with the open-sided draft tube, the optimum operating conditions correspond to the beginning of full spouting regime (2.35 times the corresponding minimum spouting velocity), and for the configuration with the nonporous draft tube the optimum point is achieved using twice the minimum spouting velocity. Moreover, a decrease in particle velocity and solid circulation is evident when very high air velocities are used, especially in the latter configuration. Therefore, use of an intermediate air velocity ($2 - 3$ times the minimum one) is suggested in those processes where a high gas-solid contact is required, since operation close to the minimum one or use of high air flow rates leads to a decrease in particle velocities and system vigorousness.

In the operation with fine particles in conical spouted beds, there is a significant increase in particle velocity in the annular zone as density and/or size are increased. Furthermore, light particles oscillate with the highest frequency in this zone, ensuring great vigorousness and so high heat and mass transfer rates in the system. This knowledge is essential for the tuning of gas and solid flow patterns, and therefore for the scaling up of this technology.

Nomenclature

AR	Aperture ratio, %
D_0	Gas inlet diameter, m
D_C	Column diameter, m
D_F	Diameter of the fountain confiner, m
D_i	Contactor base diameter, m
d_p	Average particle diameter, mm
D_T	Diameter of the draft tube, m
H	Measuring height, m
H_0	Static bed height, m
H_C	Height of the conical section, m
H_F	Distance between the bed surface and the lower end of the confiner, m
L_F	Length of the fountain confiner, m
L_H	Height of the entrainment zone of the draft tube, m
L_T	Height of the draft tube, m

R Total radius, m

r Measuring point radius, m

r/R Dimensionless radius

u velocity of the fluid at the inlet section, $m\,s^{-1}$

u_{ms} Minimum spouting velocity at the inlet section, $m\,s^{-1}$

v_s Solid velocity, $m\,s^{-1}$

Greek letters

ΔP Bed pressure drop, Pa

γ Contactor angle, $^\circ$

Acknowledgements

This work has received funding from Spain's Ministry of Science and Innovation (PID2019-107357RB-I00 (AEI/FEDER, UE)), the Basque Government (IT1218-19 and KK-2020/00107) and the European Commission (HORIZON H2020-MSCA RISE-2018. Contract No.: 823745). M. Tellabide thanks Spain's Ministry of Education, Culture and Sport for his Ph.D. grant (FPU14/05814). I. Estiati thanks the University of the Basque Country for her postgraduate grant (ESPDOC18/14).

References

[1] K. Mathur, N. Epstein, Spouted Beds, academic Edition, Academic Press Incorporated,U.S., New York, 1974.

[2] M. Olazar, M. J. San José, A. T. Aguayo, J. M. Arandes, J. Bilbao, Stable operation conditions for gas-solid contact regimes in conical spouted beds, Industrial & Engineering Chemistry Research 31 (7) (1992) 1784–1792. doi:10.1021/ie00007a025.

[3] R. C. de Brito, M. Tellabide, I. Estiati, J. T. Freire, M. Olazar, Estimation of the minimum spouting velocity based on pressure fluctuation analysis, Journal of the Taiwan Institute of Chemical Engineers 113 (2020) 56–65. doi:10.1016/j.jtice.2020.08.022.

[4] X. Chen, B. Ren, Y. Chen, W. Zhong, D. Chen, Y. Lu, B. Jin, Distribution of particle velocity in a conical cylindrical spouted bed, Canadian Journal of Chemical Engineering 91 (11) (2013) 1762–1767. doi:10.1002/cjce.21850.

[5] J. De Azevedo Barros, R. De Brito, F. Freire, J. Freire, Fluid Dynamic Analysis of a Modified Mechanical Stirring Spouted Bed: Effect of Particle Properties and Stirring Rotation, Industrial and Engineering Chemistry Research 59 (37) (2020) 16396–16406. doi:10.1021/acs.iecr.0c03139.

[6] G. Q. Liu, S. Q. Li, X. L. Zhao, Q. Yao, Experimental studies of particle flow dynamics in a two-dimensional spouted bed, Chemical Engineering Science 63 (4) (2008) 1131–1141. doi:10.1016/j.ces.2007.11.013.

[7] J. Yang, R. W. Breault, S. L. Rowan, Applying image processing methods to study hydrodynamic characteristics in a rectangular spouted bed, Chemical Engineering Science 188 (2018) 238–251. doi:10.1016/j.ces.2018.05.057.

[8] N. Epstein, J. Grace, Spouted and Spout-Fluid Beds Fundamentals and Applications, cambridge Edition, Cambridge University Press, 2011. doi:10.1017/CBO9780511777936.

[9] M. J. San José, M. Olazar, A. T. Aguayo, J. M. Arandes, J. Bilbao, Expansion of spouted beds in conical contactors, The Chemical Engineering Journal 51 (1) (1993) 45–52. doi:10.1016/0300-9467(93)80007-B.

[10] M. Cortazar, J. Alvarez, G. Lopez, M. Amutio, L. Santamaria, J. Bilbao, M. Olazar, Role of temperature on gasification performance and tar composition in a fountain enhanced conical spouted bed reactor, Energy Conversion and Management 171 (2018) 1589–1597. doi:10.1016/j.enconman.2018.06.071.

[11] M. Pozitano, S. C. Dos Santos Rocha, Fluid dynamic and polymeric coating of forest seeds of senna macranthera (collad.) irwin et barn in

conical spouted bed, Chemical Engineering Transactions 24 (2011) 667–672. doi:10.3303/CET1124112.

[12] R. Brito, R. Béttega, J. Freire, Energy analysis of intermittent drying in the spouted bed, Drying Technology 37 (12) (2019) 1498–1510. doi:10.1080/07373937.2018.1512503.

[13] M. J. San José, S. Alvarez, R. López, Catalytic combustion of vineyard pruning waste in a conical spouted bed combustor, Catalysis Today 305 (2018) 13–18. doi:10.1016/j.cattod.2017.11.020.

[14] G. Lopez, M. Olazar, M. Amutio, R. Aguado, J. Bilbao, Influence of tire formulation on the products of continuous pyrolysis in a conical spouted bed reactor, Energy and Fuels 23 (11) (2009) 5423–5431. doi:10.1021/ef900582k.

[15] J. Berghel, R. Renström, An Experimental Study on the Influence of Using a Draft Tube in a Continuous Spouted Bed Dryer, Drying Technology 32 (5) (2014) 519–527. doi:10.1080/07373937.2013.840648.

[16] T. Ishikura, H. Nagashima, M. Ide, Hydrodynamics of a spouted bed with a porous draft tube containing a small amount of finer particles, Powder Technology 131 (1) (2003) 56–65. doi:10.1016/S0032-5910(02)00321-2.

[17] H. Altzibar, I. Estiati, G. Lopez, J. F. Saldarriaga, R. Aguado, J. Bilbao,

M. Olazar, Fountain confined conical spouted beds, Powder Technology 312 (2017) 334–346. doi:10.1016/j.powtec.2017.01.071.

[18] A. Pablos, R. Aguado, M. Tellabide, H. Altzibar, F. B. Freire, J. Bilbao, M. Olazar, A new fountain confinement device for fluidizing fine and ultrafine sands in conical spouted beds, Powder Technology 328 (2018) 38–46. doi:10.1016/j.powtec.2017.12.090.

[19] M. Tellabide, I. Estiati, A. Pablos, H. Altzibar, R. Aguado, M. Olazar, New operation regimes in fountain confined conical spouted beds, Chemical Engineering Science 211 (2020). doi:10.1016/j.ces.2019.115255.

[20] M. Tellabide, I. Estiati, A. Pablos, H. Altzibar, R. Aguado, M. Olazar, Minimum spouting velocity of fine particles in fountain confined conical spouted beds, Powder Technology 374 (2020) 597–608. doi:10.1016/j.powtec.2020.07.087.

[21] J. Liu, J. R. Grace, X. Bi, Novel multifunctional optical-fiber probe: I. Development and validation, AIChE Journal 49 (6) (2003) 1405–1420. doi:10.1002/aic.690490607.

[22] M. A. Barrozo, C. R. Duarte, N. Epstein, J. R. Grace, C. J. Lim, Experimental and computational fluid dynamics study of dense-phase, transition region, and dilute-phase spouting, Industrial and Engineering Chemistry Research 49 (11) (2010) 5102–5109. doi:10.1021/ie9004892.

[23] N. Ali, T. Aljuwaya, M. Al-Dahhan, Evaluating the new mechanistic scale-up methodology of gas-solid spouted beds using gamma ray computed tomography (CT), Experimental Thermal and Fluid Science 104 (January 2018) (2019) 186–198. doi:10.1016/j.expthermflusci.2019.01.029.

[24] G. Mohs, O. Gryczka, S. Heinrich, L. Morl, Magnetic monitoring of a single particle in a prismatic spouted bed, Chemical Engineering Science 64 (23) (2009) 4811–4825. doi:10.1016/j.ces.2009.08.025.

[25] O. Gryczka, S. Heinrich, V. Miteva, N. G. Deen, J. A. M. Kuipers, M. Jacob, L. Morl, Characterization of the pneumatic behavior of a novel spouted bed apparatus with two adjustable gas inlets, Chemical Engineering Science 63 (3) (2008) 791–814. doi:10.1016/j.ces.2007.10.023.

[26] A. Atxutegi, M. Tellabide, G. Lopez, R. Aguado, J. Bilbao, M. Olazar, Implementation of a borescopic technique in a conical spouted bed for tracking spherical and irregular particles, Chemical Engineering Journal 374 (May) (2019) 39–48. doi:10.1016/j.cej.2019.05.143.

[27] G. Farnebäck, Fast and accurate motion estimation using orientation tensors and parametric motion models, Proceedings - International Conference on Pattern Recognition 15 (1) (2000) 135–139.

[28] M. Tellabide, I. Estiati, A. Atxutegi, H. Altzibar, R. Aguado, M. Olazar,

Fine particle flow pattern and region delimitation in fountain confined conical spouted beds, Journal of Industrial and Engineering Chemistry 95 (2021) 312–324. doi:10.1016/j.jiec.2021.01.006.

[29] H. Ji, A. Tsutsumi, K. Yoshida, Solid Circulation in aSpouted Bed With a Draft Tube, Chem. Eng. Jpn. 31 (1998) 842–845.

[30] H. Zhang, M. Liu, T. Li, Z. Huang, X. Sun, H. Bo, Y. Dong, Experimental investigation on gas-solid hydrodynamics of coarse particles in a two-dimensional spouted bed, Powder Technology 307 (2017) 175–183. doi:10.1016/j.powtec.2016.11.024.

[31] H. Gao, X. Gong, G. Hu, Statistical and frequency analysis of pressure fluctuation in an annular spouted bed of coarse particles, Powder Technology 317 (2017) 216–223. doi:10.1016/j.powtec.2017.05.007.

[32] M. Olazar, M. J. San José, S. Alvarez, A. Morales, J. Bilbao, Measurement of Particle Velocities in Conical Spouted Beds Using an Optical Fiber Probe, Industrial Engineering Chemistry Research 37 (4) (1998) 4520–4527.

[33] Y. L. He, S. Z. Qin, C. J. Lim, J. R. Grace, Particle velocity profiles and solid flow patterns in spouted beds, The Canadian Journal of Chemical Engineering 72 (4) (1994) 561–568. doi:10.1002/cjce.5450720402.

[34] D. L. Pianarosa, L. A. P. Freitas, C. J. Lim, J. R. Grace, O. M. Dogan, Voidage and particle velocity profiles in a spout-fluid bed, The Canadian

Journal of Chemical Engineering 78 (1) (2000) 132–142. doi:10.1002/cjce.5450780118.

[35] D. A. Santos, G. C. Alves, C. R. Duarte, M. A. S. Barrozo, Disturbances in the hydrodynamic behavior of a spouted bed caused by an optical fiber probe: Experimental and CFD study, Industrial and Engineering Chemistry Research 51 (9) (2012) 3801–3810. doi:10.1021/ie2023838.

[36] T. Djeridane, F. Larachi, D. Roy, J. Chaouki, R. Legros, Investigation of the mean and turbulent particle velocity fields in a spouted bed using radioactive particle tracking, The Canadian Journal of Chemical Engineering 76 (2) (1998) 190–195. doi:10.1002/cjce.5450760205.

[37] M. J. San José, S. Alvarez, A. Morales, M. Olazar, J. Bilbao, Solid Cross-Flow into the Spout and Particle Trajectories in Conical Spouted Beds Consisting of Solids of Different Density and Shape, Chemical Engineering Research and Design 84 (6) (2006) 487–494. doi:10.1205/cherd.05036.

[38] T. Al-Juwaya, N. Ali, M. Al-Dahhan, Investigation of cross-sectional gas-solid distributions in spouted beds using advanced non-invasive gamma-ray computed tomography (CT), Experimental Thermal and Fluid Science 86 (2017) 37–53. doi:10.1016/j.expthermflusci.2017.03.029.

[39] G. Kulah, S. Sari, M. Koksal, Particle Velocity, Solids Hold-Up, and

Solids Flux Distributions in Conical Spouted Beds Operating with Heavy Particles, Industrial and Engineering Chemistry Research 55 (11) (2016) 3131–3138. doi:10.1021/acs.iecr.5b04496.